Angular Uncertainty Refinement and Image Reconstruction Improvement in Cryo-electron Tomography

Hmida Rojbani[1,2], Étienne Baudrier[1], Benoît Naegel[1], Loïc Mazo[1] and Atef Hamouda[2]
[1]*University of Strasbourg, 67412, Illkirch CEDEX, France*
[2]*Faculty of Science of Tunis, University El-Manar, 2092, El Manar Tunis, Tunisia*

Keywords: Electron Tomography, 3*D* Structures, Tilt Angles, Angular Uncertainty, Optimization, Conjugate Gradient.

Abstract: In the field of cryo-electron tomography (cryo-ET), numerous approaches have been proposed to tackle the difficulties of the three-dimensional reconstruction problem. And that, in order to cope with *(1)* the missing and noisy data from the collected projections, *(2)* errors in projection images due to acquisition problems, *(3)* the capacity of processing large data sets and parameterizing the contrast function of the electron microscopy. In this paper, we present a novel approach for dealing with angular uncertainty in cryo-ET. To accomplish this task we propose a cost function and with the use of the nonlinear version of the optimization algorithm called Conjugate Gradient, we minimize it. We test the efficiency of our algorithm with both simulated and real data.

1 INTRODUCTION

For a better understanding of the biological cells, scientists use electron microscopy to investigate their inner structures. The cryo-ET offers the possibility to reconstruct the three dimensional (3*D*) volume of a cell slice. The cryo-ET principle is to acquire two dimensional (2*D*) projections with the **T**ransmission **E**lectron **M**icroscope (TEM) by tilting the sample around an axis (*cf.* Figure 1). The tilting range is $[-70°, 70°]$ with steps between $2°$ and $5°$. Then the projection angles are known and are used in the reconstruction of the 3*D* sample. Figure 2 presents the four different steps of cryo-ET.

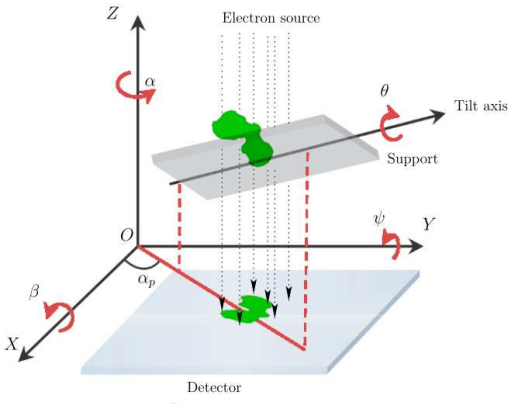

Figure 1: Transmission electron microscopy acquisition mechanism.

Nevertheless, there are several limits to the resolution of the reconstruction: the missing data corresponding to the uncovered projection space, the low electron dose used during the acquisition to minimize the weight of radiation damage (Egerton et al., 2004), the thickness of the ice used in the sample fixation that affects also the final reconstructed volume resolution (Stagg et al., 2006) and the error made on the projection parameters. The missing data, the electron dose and the ice thickness are an acquisition phase problem that we cannot correct them directly in our work, but we try to minimize their effect on the reconstruct results. The classical reconstruction process involves as a first step an image alignment process. The two well common alignment techniques are (Frank, 2006): *(1)* marker tracking, where gold particles are implanted into the samples before the acquisition of the images and then the calculation based on these markers is used to align the images (Brandt and Ziese, 2006), (Sorzano et al., 2009); *(2)* cross-correlation methods, where alignment is carried out by the cross-correlation calculation between each successive couple of images (Zheng et al., 2010).

The second step of the cryo-ET is the 3*D* reconstruction. Numerous reconstruction methods are used in cryo-ET, mainly belonging to two families. First, the analytic family, with methods as filtered back-projection or direct Fourier inversion, implemented in Fourier's space (Penczek, 2010). The second family is the algebraic family, with iterative real-

Rojbani, H., Baudrier, É., Naegel, B., Mazo, L. and Hamouda, A.
Angular Uncertainty Refinement and Image Reconstruction Improvement in Cryo-electron Tomography.
DOI: 10.5220/0005680600940100
In *Proceedings of the 11th Joint Conference on Computer Vision, Imaging and Computer Graphics Theory and Applications (VISIGRAPP 2016) - Volume 3: VISAPP*, pages 96-102
ISBN: 978-989-758-175-5

space methods such as ART (Gordon et al., 1970) or SIRT (Gilbert, 1972).

Besides the reconstruction difficulties, the acquisition process rises different type of problems such as the specimen movement (translation, rotation) over the carbon support especially when the tilting reaches the highest values, the blur caused by the **C**ontrast **T**ransfer **F**unction (CTF), and the uncertainty on the angular information due to mechanical imprecision of the microscope (Colliex, 1998). All these problems affect the quality of resolution of the reconstructed object. Many approaches are proposed to overcome all this mentioned problems except for the angular uncertainty, due to the fact that the resolution of the reconstruction is mediocre, so the angular uncertainty does not have the effect over it. Now days, and due to the improvement of the reconstruction techniques, the resolution become important especially when we aim to reconstruct and locate small particles such as ribosome and nucleosomes. Treating the angular uncertainty will push as forward to a better reconstruction resolution.

We begin in our work by concentrating on the angular uncertainty problem, which we prove in our tests that even a slight change in the set of angles use in the reconstruction has its affect over the accuracy of the resolution of the reconstructed 3*D* volume. Our approach is based on optimization problem where we use a cost function has the set of angles as parameters to be minimized. To gain more accuracy we include also the reconstructed object as parameters into the function. Using the two sets of parameters simultaneously in our approach provides more accurate results than optimizing the angular uncertainty and the reconstructed object separately.

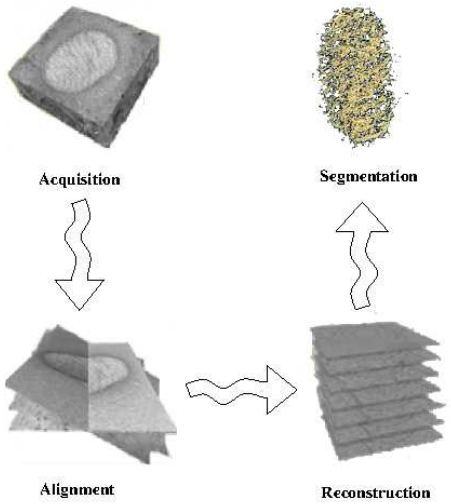

Figure 2: Different Steps of cryo-ET.

2 RELATED WORK

In recent years, the use of simultaneous optimization is increased in many fields. One of those fields is the alignment phase in the reconstruction. For example, in the field of the singular particles reconstruction, a large set of small projections used in the reconstruction of an object are from unknown orientations. Thus, to improve the estimation of the unknown projection orientations, Yang *et al.* (Yang et al., 2005) proposed to use a Quasi-Newton optimization based algorithm to minimize a cost function between the projection angles and the reconstructed 3*D* object starting from a rough reconstruction.

In cryo-ET, the context is different: the data is a small set of large projections with known tilt angles. However, this tilt angles can be erroneous due to the malfunction of the tilt mechanism of the object holder in the TEM. In this field, Tran *et al.* (Tran et al., 2013) proposed a hierarchical method to correct the reconstruction and the alignment problems in alternating way. They treat the transformation parameters (translation, rotation, scale). Inspiring from the cross-correlation method of alignment, they begin by finding the first set of transformation parameters by an optimization between each successive pair of projection images. After that, a first reconstruction is applied followed by refinement of the set of transformation. If the method has not yet converged, they raise a new reconstruction. Infact, the reconstruction is based on an optimization between the actual projections and the resulting projections of the reconstructed object. In the same way, the phase of refinement of transformation parameters represents an optimization between the processing parameters found from the current projections and those of the previous iteration.

We propose in our work to optimize the reconstructed object and the transformation parameters simultaneously at the same level. In addition, we take into account the error of the angular uncertainty of projection. Indeed, we make the correction on the reconstructed object itself, instead of those made on projections. The idea is to try for each projection orientation used to reproduce the same projection provided by the TEM. In this paper, we only present our work for the refinement of the projection angles and the reconstructed object.

The rest of the paper is structured as follows: in Section 3, the projection algebraic model of the acquisition is given; in Section 4, the proposed approach is detailed and the associated cost function is defined; the results are shown and discussed in Section 5. Finally, we summarize and give some perspectives.

3 PROJECTION ALGEBRAIC MODEL

In the cryo-ET, The reconstruction is three-dimensional problem, but in the section we will give a general *n*-dimensional presentation for the problem. To see the reconstruction problem as an algebraic model, we must change the reconstructed volume f and the projections images p_i to their respective vectors forms.

Let $\mathbf{f}$ be the vector representation of *n*-dimensional image f, $\mathbf{f} = (\mathrm{f}_1, \mathrm{f}_2, \ldots, \mathrm{f}_{\mathbf{N}})^T$. $\mathbf{N}$ is the number of voxels of $\mathbf{f}$, in other words $\mathbf{N} = \Pi_{d=1}^{n} N_d$, where N_d is the size of f in the dimension d.

Let $\mathbf{p}^{\theta_i} = (\mathrm{p}_1^{\theta_i}, \mathrm{p}_2^{\theta_i}, \ldots, \mathrm{p}_{\mathbf{M}}^{\theta_i})^T$ is the vector representation of the $n-1$-dimensional projection image p_i of the image f according to the orientation θ_i. $\mathbf{M}$ is the number of pixels of $\mathbf{p}$, in other words $\mathbf{M} = \Pi_{d=1}^{n-1} M_d$, where M_d is the size of p_i in the dimension d.

In fact, $\mathbf{p}$ is an element of a bigger vector $\mathbf{P}$, which contains all the elements of the $\mathbf{S}$ projections images. $\mathbf{S}$ is the numbers of the angles used in the tilting process. We can assemble these angles in a set called Θ, and then we have $\mathbf{P} = (\mathbf{p}^{\theta_1}, \mathbf{p}^{\theta_2}, \ldots, \mathbf{p}^{\theta_i}, \ldots, \mathbf{p}^{\theta_\mathbf{S}}),\ \forall \theta_i \in \Theta$.

We define the relation between the projection vector $\mathbf{P}$ and the image vector $\mathbf{f}$ as:

$$\mathbf{P} = W\mathbf{f}, \tag{1}$$

Which can be seen also as :

$$\mathbf{p}^{\theta_i} = W_{\theta_i}\mathbf{f}, \tag{2}$$

Thereby, the projection problem is modeled as an equation system whose matrix W_{θ_i} is sparse. The matrix W_{θ_i} holds the coefficients of the projections according to the angle θ_i. In fact, each line of this matrix describes one of the projection lines passing throws the image. Many methods are proposed to calculate this matrix such as "voxel driven" and "ray driven" (Joseph, 1982). However, in our work, the calculation of W_{θ_i} is based on the "distance driven" method proposed by (Man and Basu, 2004). Note that the non null coefficients change when θ_i changes but the matrix W_{θ_i} remains sparse. The equation (2) cannot be straightly inversed. Then we propose thereafter a reconstructed volume refinement method that simultaneously acts on the reconstructed volume and the tilt angles.

4 PROPOSED APPROACH

When we investigate the reconstruction problem, we find that the only real data that we have it is the projections images and a set of uncertain angles of projection. Hence, the idea to create a function that can calculate the difference or we can call it also the distance between the real projection data and the projection data found after re-projecting the reconstructed volume according to the current set of angles. Thus, by refining these two, we can assure having a much accurate reconstructed objet.

We begin by defining the cost function $\mathcal{C}$, which presents the Euclidian distance between the real set of projection data $\mathbf{\Pi}$ and the re-projection data from the reconstructed object $\mathbf{P}$, so we have :

$$\mathcal{C}(\mathbf{f}, \Theta) = \frac{1}{2}\|\mathbf{\Pi} - \mathbf{P}\|_2^2 = \frac{1}{2}\sum_{i=1}^{\mathbf{S}} \|\boldsymbol{\pi}^i - \mathbf{p}^{\theta_i}\|_2^2 \tag{3}$$

This equation can be developed to :

$$\mathcal{C}(\mathbf{f}, \Theta) = \frac{1}{2}\sum_{i=1}^{\mathbf{S}}\sum_{j=1}^{\mathbf{M}} (\pi_j^i - \mathrm{p}_j^{\theta_i})^2 \tag{4}$$

$$= \frac{1}{2}\sum_{i=1}^{\mathbf{S}}\sum_{j=1}^{\mathbf{M}} (\pi_j^i - \sum_{k=1}^{\mathbf{N}} w_k^{\theta_i, j}\mathrm{f}_k)^2 \tag{5}$$

where $w_k^{\theta_i, j}$ is the projection coefficient of the k-th pixel by the j-th projection line according to the θ_i.

The cost function $\mathcal{C}$ depends on three parameters, the actual projections, the current reconstructed volume and the current tilt angles.

We use the square in the equation (3) to ensure the positivity of the function. The similarity between the two types of projections reaches its maximum when the function $\mathcal{C}$ reaches its minimum. In this case, the solution set of our problem $(\widehat{\mathbf{f}}, \widehat{\Theta})$ is :

$$(\widehat{\mathbf{f}}, \widehat{\Theta}) = \operatorname{argmin}\ \mathcal{C}(\mathbf{f}, \Theta) \tag{6}$$

The equation (6) is convex in $\mathbf{f}$ (due to the using of a quadratic sum) and Θ is close to the solution by hypothesis . We can therefore assume that in this case, the optimization problem of Eq. (6) is convex. Moreover, it is plain that the cost function $\mathcal{C}$ is not linear according to $(\mathbf{f}, \Theta)$. Thus, we have to use a non-linear minimization algorithm. Among the known deterministic optimization algorithms mentioned in the literature (Nocedal and Wright, 2006), we chose the non-linear version of the **C**onjugate **G**radient (CG) algorithm (Dai and Yuan, 1999). The CG method is the most prominent iterative method for solving sparse systems of equations. We preferred this algorithm for its convergence rate, its simple implementation and since it appeals only to the first order derivative.

The steps below constitute one of the CG iteration of movement along a conjugate direction d_i. The algorithm starts by initializing $d_0 = g_0 = -\nabla\mathcal{C}(\chi_0)$ (Dai and Yuan, 1999), then :

- find α_i the length of the descent step that minimizes $\mathcal{C}(\chi_i + \alpha_i d_i)$,
- $\chi_{i+1} = \chi_i + \alpha_i d_i$,
- $g_{i+1} = -\nabla\mathcal{C}(\chi_{i+1})$,
- $\beta_i = \max\{\frac{g_{i+1}^T(g_{i+1}-g_i)}{g_i^T g_i}, 0\}$,
- updating the conjugate direction $d_{i+1} = g_{i+1} + \beta_i d_i$.

The first step to use the CG is to calculate the gradient of our cost function $\mathcal{C}$. In order to facilitate this phase, we have changed the equation (4) by :

$$\mathcal{C}(\mathbf{f},\Theta) = \frac{1}{2}\sum_{i=1}^{\mathbf{S}}\sum_{j=1}^{\mathbf{M}}(\mathcal{C}r(\mathbf{f},\theta_i,j))^2 \qquad (7)$$

with $\mathcal{C}r(\mathbf{f},\theta_i,j) = \pi_j^i - \sum_{k=1}^{\mathbf{N}} w_k^{\theta_i,j}\mathrm{f}_k$.

Now we calculate the $\nabla\mathcal{C}r$ then we will deduct the $\nabla\mathcal{C}$. Due to the discrete nature of the cost function, we use the finite difference to estimate the gradient values.

For $h = 1,\ldots,\mathbf{N}$, the f_h-th partial derivative of $\mathcal{C}$ is given by

$$\frac{\partial\mathcal{C}r}{\partial\mathrm{f}_h} = -w_h^{\theta_i,j}$$

which leads to,

$$\frac{\partial(\mathcal{C}r)^2}{\partial\mathrm{f}_h} = -2w_h^{\theta_i,j}\left(\pi_j^i - \sum_{k=1}^{\mathbf{N}} w_k^{\theta_i,j}\mathrm{f}_k\right).$$

Then,

$$\frac{\partial\mathcal{C}}{\partial\mathrm{f}_h} = -\sum_{i=1}^{\mathbf{S}}\sum_{j=1}^{\mathbf{M}} w_h^{\theta_i,j}\left(\pi_j^i - \sum_{k=1}^{\mathbf{N}} w_k^{\theta_i,j}\mathrm{f}_k\right).$$

In the same, we have for the h-th derivative according to Θ, $\forall h = 1,\ldots,\mathbf{M}$.

$$\frac{\partial\mathcal{C}r}{\partial\theta_h} = \frac{1}{2\Delta_\theta}\left(\sum_{k=1}^{\mathbf{N}}(w_k^{(\theta_h-\Delta_\theta),j} - w_k^{(\theta_h+\Delta_\theta),j})\mathrm{f}_k\right)$$

where $w_k^{(\theta_h+\Delta_\theta),j}, w_k^{(\theta_h-\Delta_\theta),j}$ are the projection coefficients according to $\theta_h+\Delta_\theta, \theta_h-\Delta_\theta$, Δ_θ here is the finite difference used in the gradient calculation. which leads to,

$$\frac{\partial(\mathcal{C}r)^2}{\partial\theta_h} = \frac{1}{\Delta_\theta}\left(\sum_{k=1}^{\mathbf{N}}(w_k^{(\theta_h-\Delta_\theta),j} - w_k^{(\theta_h+\Delta_\theta),j})\mathrm{f}_k\right) \times \left(\pi_j^i - \sum_{k=1}^{\mathbf{N}} w_k^{\theta_i,j}\mathrm{f}_k\right).$$

Then,

$$\frac{\partial\mathcal{C}}{\partial\theta_h} = \frac{1}{2\Delta_\theta}\sum_{j=1}^{\mathbf{M}}\left(\sum_{k=1}^{\mathbf{N}}(w_k^{(\theta_h-\Delta_\theta),j} - w_k^{(\theta_h+\Delta_\theta),j})\mathrm{f}_k\right) \times \left(\pi_j^i - \sum_{k=1}^{\mathbf{N}} w_k^{\theta_i,j}\mathrm{f}_k\right).$$

We noticed that according a small value to the parameter Δ_θ may produce a null derivative for some angles because of the discrete nature of the rotation which may boil down to the identity map for the small angle changes. Therefore, after many experiments we found that the most suitable value is 1°.

After computing the gradient, we can proceed to the optimization phase. Firstly, we reconstruct the initial object; in our case, we chose to use the algebraic reconstruction method SIRT for this phase. However, any algorithm either analytic or algebraic is can be used. Secondly, we take the initial reconstructed object and the projection data with the tilt angles used in the acquisition as input for the iterative CG algorithm. The algorithm of our approach is showed in Alg.1.

Algorithm 1: CG refinement algorithm.

initialization $\mathbf{f}_0 = \mathbf{f}^{init}, \Theta_0 = \Theta^{init}$, cond=0
while $iter < iter_{max}$ AND cond=0 **do**
  compute gradient $\nabla\mathcal{C}(\mathbf{f}_{\text{iter}}, \Theta_{\text{iter}})$
  compute $\mathbf{f}_{\text{iter}+1}, \Theta_{\text{iter}+1}$ with the CG
  $\Delta\mathcal{C} = \mathcal{C}(\mathbf{f}_{\text{iter}}, \Theta_{\text{iter}}) - \mathcal{C}(\mathbf{f}_{\text{iter}+1}, \Theta_{\text{iter}+1})$
  if $\Delta\mathcal{C} < \varepsilon$ **then**
    cond=1
  end if
  $\mathbf{f}_{\text{iter}} \leftarrow \mathbf{f}_{\text{iter}+1}, \Theta_{\text{iter}} \leftarrow \Theta_{\text{iter}+1}, iter \leftarrow iter+1$
end while
return $\mathbf{f}_{\text{iter}+1}$, $\Theta_{\text{iter}+1}$

5 RESULTS

Several experiments were conducted to assess the efficiency of the proposed method on $2D$ and $3D$ data. The tilt angles used for $2D$ tests are between -70° and 70° with a 2° tilt step. For each angle a random error in $[-1.5^\circ\ 1.5^\circ]$ is added. For the $3D$ tests, We used a different set of angles, one similar to the set used in cryo-ET. The boundaries are the same, but the tilt step is different. The step used between -50° and 50° is 5° and it is 2° for the others. One can notes that the number of tilt angles for the $3D$ case is less than the $2D$, which makes the refinement harder. Along the projection noise, we used three sets of tilt angles: the real one, one with absolute value of the random error $\leq 1^\circ$ and one with random error $\leq 2^\circ$.

To measure the quality of reconstruction, we propose two evaluation criteria. The first is the cross-correlation coefficient (equation (8)). It is a criterion to measure the degree of similarity between the original image and the reconstructed image. This coefficient is equal to 1 when the reconstructed image coincides exactly with the original image and zero otherwise. The second criterion is **N**ormalized **R**oot **M**ean **S**quare **E**rror (*NRMSE*) defined by the equation (9). Unlike the correlation coefficient, the zero of the NRMSE means a better result. We use *NRMSE* to measure the quality of angles correction produced by our approach. The equation (10) shows the **M**easure of **A**ngle **C**orrection (*MAC*). More the *MAC* value is close to zero, the more the angles found by our approach are corrects.

$$Corr = \frac{\sum_{k=1}^{\mathbf{N}}(\mathrm{f}_k - M(\mathbf{f}))(\widehat{\mathrm{f}_k} - M(\widehat{\mathbf{f}}))}{\sqrt{\sum_{k=1}^{\mathbf{N}}(\mathrm{f}_k - M(\mathbf{f}))^2 \sum_{k=1}^{\mathbf{N}}(\widehat{\mathrm{f}_k} - M(\widehat{\mathbf{f}}))^2}} \quad (8)$$

$$NRMSE = \frac{\sqrt{\frac{\sum_{i=1}^{\mathbf{S}}(\theta_i - \widehat{\theta_i})^2}{S}}}{\max(\Theta) - \min(\Theta)} \quad (9)$$

$$MAC = 1 - \frac{NRMSE_{init} - NRMSE_{final}}{NRMSE_{init}} \quad (10)$$

With $NRMSE_{init}$ and $NRMSE_{final}$ are respectively the *NRMSE* between the true angles, the angles before the optimization and the angles after the optimization. Thus, if the angles after the optimization are totally corrected $NRMSE_{final}$ will be zero, which means the *MAC* will be zero also. However, if the errors are not corrected or even are amplified, the *MAC* will be greater than 1.

The 2*D* experiments involve 122 2*D* synthetic gray-level images randomly generated at different resolutions $N \times N$ with $N = 32, 64, 128, 256, 512$. A sample of the synthetic images used are shown in the figure 3. The same number of iterations are applied on all the experiments images.

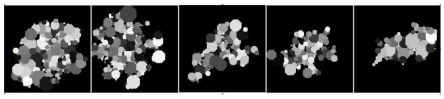

Figure 3: 2*D* synthetic images.

All the projections were corrupted with different levels of Gaussian noise σ and a random error has been assigned to each of the tilt angles (some samples are shown in Fig. 5).

The mean results of the synthetic data are gathered in Tab. 1 and the tilt angles refinements of one of the tests are presented in Fig. 4.

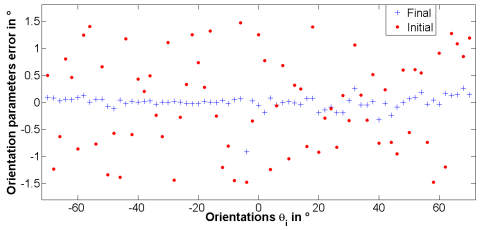

Figure 4: Error enhancement between the original tilt angles and the corrected ones for one of the test images.

For all the tested resolutions, the error that remains after optimization is under 30% of wrong pixels and under 20% of wrong projection angles. In our future work, we will investigate deeper the relation between the image size and the number of iterations to reach the minimum. We notice also that more the gray-levels we use, more the discrete research space is connected and more the method is robust to noise.

Table 1: Evaluation of 2*D* synthetic data.

Noise variance σ	0	2	4	6	8
Corr	0.97	0.93	0.88	0.87	0.83
MAC	0.09	0.12	0.15	0.18	0.19

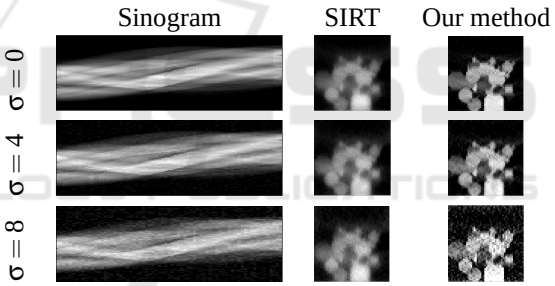

Figure 5: The sinogram of a single image is corrupted with Gaussian noise of different variances σ. The reconstruction by SIRT (Penczek, 2010) and our method is shown for each noise level.

The 3D experiments were done on synthetic and real data. A set of 3D synthetic gray-level volumes were created with different resolutions ($N = 16, 32, 64, 128$). Fig. 7 shows a 3*D* volume with its results. The real data are projections of the Orf-parapoxvirus: Fig. 6: presents some of those projections.

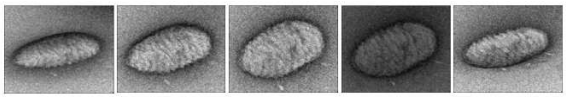

Figure 6: Orf-parapoxvirus projections respectively according to the angles -60°, -40°, -10°, 20°, and 50°.

The mean results according to deferent angular error (*AE*) and noise variance σ sing the same evalua-

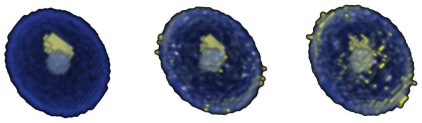

Figure 7: Reconstruction of a synthetic 3D; *left:* 3D volume ($N = 32$), *center:* with our method and *right:* with SIRT.

tion measures used for the 2*D* evaluation are given in the Tab. 2 and Tab. 3.

In this two table, one can notice the promising results, the correlation is very high over all the testing seniors. The same for the *MAC* results that are low for the most of the testing seniors. We notice also, that when we use the true angles, they are slightly corrupted by our algorithm.

Table 2: *Corr* results for 3*D* synthetic data.

σ \ *AE*	0°	≤ 1°	≤ 2°
0.5	0.97	0.89	0.88
2	0.90	0.84	0.85
5	0.88	0.77	0.75

Table 3: *MAC* results for 3*D* synthetic data.

σ \ *AE*	0°	≤ 1°	≤ 2°
0.5	0.01	0.09	0.08
2	0.05	0.13	0.14
5	0.07	0.18	0.21

For the Orf-parapoxvirus reconstruction, we calculate the improvement rate of resolution, which was 21.86%, which we think it is a good result considering that we used volume and angular refinement only. Also, we sought an opinion of an expert in the biology field and he validate the amelioration of the reconstruction object generated by our approach. Some of the 2D slice of the reconstructed object by our approach and SIRT are presented in Tab. 4.

Table 4: Some of the 2*D* slices of the reconstructed object by SIRT and our approach.

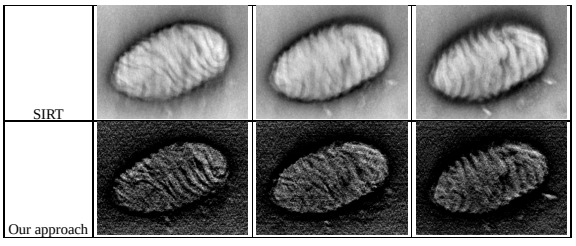

6 CONCLUSION

In this paper, we have described a method to refine the reconstruction of an object from a set of its tomographic projections and simultaneously correct the errors over the used tilt angles. The starting point of the proposed method is an approximation of the object (provided by some reconstruction algorithm) together with a set of uncertain tilt angles used to acquire the projections. Then, considering both the angles and the values of the reconstructed volume as parameters, we minimize the Euclidean distance between our ground truth (the original tomographic projections) and the re-projections of the estimated object according to the current corrected set of angles. For the optimization process, a non-linear conjugate gradient algorithm is used. Our experiments shows that the proposed method improves the reconstruction of the object compared to using SIRT directly. Further improvements of the reconstruction can still be obtained in the frame of our method. In our future work, we plan also to incorporate the other transform parameters of the alignment process, also, the correction of the contrast transfer function in the optimization process.

REFERENCES

Brandt, S. and Ziese, U. (2006). Automatic TEM image alignment by trifocal geometry. *Journal of Microscopy*, 222:1–14.

Colliex, C. (1998). *The Electron Microscopy*. Presses Universitaires de France.

Dai, Y. H. and Yuan, Y. (1999). A nonlinear conjugate gradient method with a strong global convergence property. *SIAM J. on Optimization*, 10(1):177–182.

Egerton, R., Li, P., and Malac, M. (2004). Radiation damage in the TEM and SEM. *Micron*, 35(6):399–409.

Frank, J. (2006). *Electron tomography: methods for three-dimensional visualization of structures in the cell*. Springer.

Gilbert, P. (1972). Iterative methods for the three-dimensional reconstruction of an object from projections. *Journal of Theoretical Biology*, 36(1):105–117.

Gordon, R., Bender, R., and Herman, G. (1970). Algebraic Reconstruction Techniques (ART) for three-dimensional electron microscopy and X-ray photography. *J Theor Biol*, 29(3):471–481.

Joseph, P. (1982). An improved algorithm for reprojecting rays through pixel images. *Medical Imaging, IEEE Transactions on*, 1(3):192–196.

Man, B. D. and Basu, S. (2004). Distance-driven projection and backprojection in three dimensions. *Physics in Medicine and Biology*, 49(11):2463.

Nocedal, J. and Wright, S. (2006). *Numerical Optimization*. Springer Series in Operations Research and Financial Engineering. Springer-Verlag New York, 2 edition.

Penczek, P. (2010). Chapter one - fundamentals of three-dimensional reconstruction from projections. In Grant, J., editor, *Cryo-EM, Part B: 3-D Reconstruction*, volume 482 of *Methods in Enzymology*, pages 1–33. Academic Press.

Sorzano, C., Messaoudi, C., Eibauer, M., Bilbao-Castro, J., Hegerl, R., Nickell, S., Marco, S., and Carazo, J. (2009). Marker-free image registration of electron tomography tilt-series. *BMC Bioinformatics*, 10(1):124.

Stagg, S., Lander, G., Pulokas, J., Fellmann, D., Cheng, A., Quispe, J., Mallick, S., Avila, R., Carragher, B., and C.S.Potter (2006). Automated cryo-em data acquisition and analysis of 284742 particles of groel. *J Struct Biol*, 155:470–481.

Tran, V.-D., Moreaud, M., Thiébaut, E., Denis, L., and Becker, J. M. (2013). Inverse Problem Approach for the Alignment of Electron Tomographic Series. *Oil & Gas Science and Technology - Revue d'IFP Energies nouvelles*, 69(2):279–291.

Yang, C., Ng, E., and Penczek, P. (2005). Unified 3-D structure and projection orientation refinement using quasi-Newton algorithm. *J Struct Biol*, 149(1):53–64.

Zheng, Q., Sedat, J., and Agard, D. (2010). Automated data collection for electron microscopic tomography. *Methods in Enzymology*, 481(10):283–315.